Case Studies in Chemical and Environmental Engineering 11 (2025) 101048

Contents lists available at ScienceDirect

Case Studies in Chemical and Environmental Engineering

journal homepage: www.sciencedirect.com/journal/case-studies-in-chemical-and-environmental-engineering

Case Report

Prospect for pico-hydropower generation from 3D printed Polyethylene Terephthalate Glycol (PETG) Polymer: A Case Study in Pusu River, Malaysia

Nuranisa Suhada binti Abd Rahim [a], Chuan Choong Yang [a,*], Nor Aiman Sukindar [b]

[a] Department of Manufacturing and Materials Engineering, Faculty of Engineering, International Islamic University Malaysia, Kuala Lumpur, 50728, Malaysia
[b] School of Design, Universiti Teknologi Brunei, Jalan Tungku Link Gadong, BE1410, Brunei Darussalam

ARTICLE INFO

Keywords:
Archimedean screw turbine (AST)
3D printing
Polyethylene Terephthalate Glycol (PETG)
Tensile strength
Torque generation

ABSTRACT

In Malaysia, rural communities rely on fossil fuel-powered generators for electrification. A small-scale Archimedean Screw Turbine (AST) can be utilized to generate pico-hydropower for potential clean energy generation. However, no study focuses on investigating the strength and torque of 3D printed AST with Polyethylene Terephthalate Glycol (PETG) polymer. Hence, the aim of this work is to investigate the mechanical strength and torque generation of 3D printed PETG AST through Ultimate Tensile Strength (UTS) test and experimental test. UTS test results show that 37.10MPa is the highest tensile strength obtained while 0.0195Nm is the optimum torque generated through AST experimental test.

1. Introduction

In Sarawak, Malaysia, 20 % of rural communities in that state still suffering electric poverty [1] that cause majority of villagers still depends on fossil fuel-powered generators for electrification [2]. Instead of using fossil fuel-powered generators, renewable energy technology should be adopted as it can assist in reducing pollution and improving environmental quality [3]. In Malaysia, the potential renewable energy to be used is hydropower as it has lots of river especially in Sarawak which most of the rivers in Sarawak operates in low flow velocity [2]. Therefore, Archimedean Screw Turbine (AST) would be one of the alternatives to develop pico-hydro plant (generate power below than 5KW) as it is capability to operate under low flow [4]. Thus, objective of this work is to study the feasibility of small-scale AST to generate pico-hydropower energy.

2. Literature review

2.1. Archimedean Screw Turbine (AST) design

Archimedean Screw Turbine (AST) can be utilized as pico-hydropower generator which was able to generate power below than 5kW utilizing low head level (difference between upper water and lower water level elevation at less than 10 m) and low flow rate (below 10 m^3/s). However, the performance of the AST was influenced by its geometry [4] as shown in Fig. 1.

For AST designs, there are various research work performed to study the performance of this turbine to harvest energy. Table 1 shows the summary of the AST research contributions.

From the findings, it indicates that lack studies in the performance of the diameter ratio of AST to generate the torque. This is because majority researchers used only one fixed value of diameter ratio. Thus, in this work, the study focusses to investigate the performance of the diameter ratio in influencing the generation of torque.

2.2. Archimedean Screw Turbine (AST) fabrication methods for pico-hydro power generations

Complex geometry of AST makes fabrication difficult, which slows the adoption of this technology. Currently, the process to fabricate AST using steel (traditional manufacturing process) is complex and lengthy as it involves bending and welding process [10]. Therefore, the current method is not environmentally friendly as this process consumes lots of energy and less energy efficiency [11]. Due to this, it encouraged researchers to explore different methods and materials to fabricate AST. Complex geometries are impossible or very difficult to produce using

* Corresponding author.
E-mail address: yangcc@iium.edu.my (C.C. Yang).

https://doi.org/10.1016/j.cscee.2024.101048
Received 20 October 2024; Received in revised form 23 November 2024; Accepted 4 December 2024
Available online 11 December 2024

traditional manufacturing process [12]. Furthermore, additive manufacturing process is environmentally friendly with low energy consumption [13] and less material waste generated [12]. This process also was widely being used in aerospace, automotive and medical industry [12].

Generally, additive manufacturing is a process where the parts are created layer by layer deposition which is digitally controlled. Additive manufacturing also known as 3D printing process or rapid prototyping process [12]. In this manufacturing process, the common polymer materials used are Polyactic Acid (PLA) and Polyethylene Terephthalate Glycol (PETG) [14].

In AST fabrication, 3D printing process also was used by other researchers to investigate their AST performance. As an example, Lee et al. [15] utilized 3D printing process to fabricate AST using PLA material to validate the geometric of controllable pitch Archimedean Screw Turbine. In conducting the experimental test, Zitti et al. [16] also applied 3D printing process in their work and PLA was used to investigate the performance of their AST.

From the above findings, majority of the researchers focus on validating the geometric of the AST's model with PLA material. However, no further investigation on the strength of 3D printed AST to validate the feasibility to generate torque. Hence, this work focusses to study the strength and torque of 3D printed AST utilizing PETG material as potential clean energy generation. Instead of using PLA material, PETG material was selected due to its water resistance characteristics [17].

2.3. Effect of infill density on 3D printed components' strength

The final products of 3D printed parts do not only depend on the material itself but also have been influenced by the printing parameters [18]. Infill density defines as the percentage of volume inside of the object that filled by the extruded filament material. If there is no material filled within the inner volume, air will take this space. The value of infill density is in a range of 0 %–100 %. 0 % infill density represents that the inner volume is hollow meanwhile the 100 % infill density shows that the inner volume totally filled [19].

Parameters of infill density mainly effects the mechanical properties of the 3D printed products. Ambati and Ambatipudi (2022) [19] also conduct a study on investigating the mechanical properties of PLA polymer by varying the infill pattern and infill density. 60 %, 75 % and 90 % infill densities has been tested in this research work. The results shows that infill density of 90 % has the highest strength. In accordance with a study conducted by Maszybrocka et al. (2022) [20], the strength properties raised as the filling density increased. According to Farbman and McCoy, filling density can be altered according to the intended use of the application of product (Farbman & McCoy,2016) [21].

Table 1
Summary of the AST research contributions.

References	Main Contributions
Lee and Lee [2]	• Performed experimental test used 1 number of blade of AST with fixed diameter ratio of 0.5 at low flow rate from 0.3 to 1.7 L/s by varying angle at high inclination angle from 30° to 90°. • 45° was optimum inclination angle at all flow rate and generated the highest torque of 0.9 N.m at 100L/min flow rate.
Erinofiardi et al. [5]	• Conducted test used 1 blade of AST at flow rate 1.2 L/s by varying inclination angle at 22°, 30° and 40°. • 22° was optimum inclination angle and generated the highest torque at 0.13 N.m.
Syam et al. [6]	• Conducted experimental test for AST at 30° inclination angle by varying flow rate at 3, 9 and 20 L/s using their AST with geometry of N = 1 and diameter ratio = 0.54. • AST generated the highest torque of 4 N.m at 20 L/s.
Maulana et al. [7]	• Performed experimental test for AST at 30° inclination angle by varying flow rate at 4.4, 12.5 and 25 L/s using their AST with geometry of N = 2 and 0.54 diameter ratio. • Findings indicates that at high flow rate of 25 L/s generated the highest torque at 5 N.m.
Nagel [8]	• In designing Archimedean screw, he suggests that the dimension of the diameter ratio needs to be 0.45 to 0.55.
Abd Rahim, N.S. et al. [9]	• AST's optimum design was 3 blades and an inclination angle of 38° to generate highest torque at 0.046 Nm from flow velocity of 0.06 m/s.

In this work, infill density that will be employed for PETG polymer in a range of 50 %–80 % with steps of 10 % in order to investigate how this parameter affects the strength of AST.

2.4. Effect of printing speed on 3D printed components' strength

Miazio (2019) [22] has studied the strength of PLA polymer by varying printing speed of 3D printer. The speed was varied from 20 to 100mm/s. The research shows that increasing the printing speed will reduce the strength of samples. To print PLA polymer, range of 50–80 mm/s are the best printing speed values as it indicates the strength of specimens remains at constant level. The average of breaking force for printing speed of 50, 60, 70 and 80mm/s are 0.56KN, 0.57KN, 0.55KN and 0.55KN respectively. Nevertheless, printing speed that above than 80mm/s, it shows that the strength of samples declines significantly.

Hsueh et al. (2021) [23] has performed research on the effect of two different printing parameters which are printing speed and printing temperature on PLA polymer and PETG polymer. The printing speed for PLA polymer was varied from 35 to 45 mm/s while for PETG polymer was varied from 25 to 35mm/s. The research indicates that the strength

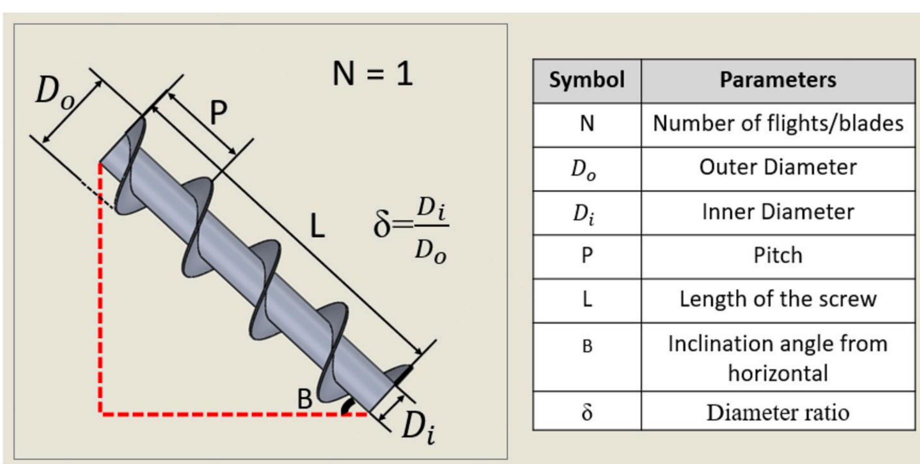

Fig. 1. Archimedean screw turbine parameters.

of PLA polymer is increasing with increasing of printing speed meanwhile for PETG polymer, it indicates vice versa.

Therefore, in this work, printing speed that will be employed for PETG polymer in a range of 20–60 mm/s in order to investigate how printing speed will influence the strength of AST.

3. Methodology

Overall methodology of this work is shown in Fig. 2.

From Fig. 2, this work was divided into two tests which are strength test and AST experimental test. Details of each test was discussed in section 3.1 and 3.2 respectively.

3.1. Strength test

Ultimate tensile Strength (UTS) test was carried out to study the mechanical strength of 3D printed PETG polymer. Details of the strength test for 3D printed PETG was discussed in section below.

3.1.1. Experimental setup for Ultimate Tensile Strength (UTS) test for 3D printed PETG

Ultimate Tensile Strength (UTS) experimental test was performed to investigate the mechanical strength of 3D printed PETG. The specimen needs to be designed according to the ASTM D638- Type 1 standard using SolidWorks software. Then, the specimens were fabricated via 3D printing process using different parameters settings. The parameters settings are Printing Speed (mm/s) with values of 20, 30, 40, 50 and 60 respectively and Infill density (%) with values of 50, 60, 70 and 80 respectively. Three specimens were printed for each variable parameter. Ultimaker Cura 5.5.0 software was used to slice specimens according to the parameter's settings as shown in Table 2.

Creality Ender Pro Max 3 printer, with 0.8 mm hardened steel nozzle was used to print these specimens. PETG filament (manufactured by e-sun) with diameter of 1.75 mm was used in this work. Next, the fabricated samples were used for UTS test to investigate the effect of printing speed and infill density on tensile strength. Ultimate Tensile Machine was used to perform tensile strength on 3D printed specimens as shown in Fig. 3.

Fig. 3 illustrates the process to perform UTS test which is the specimen needs to be placed within the UTS machine gripper.

3.1.2. Data analysis using the two-factor Analysis of Variance (ANOVA) and tukey test for infill density and 3D printing speed parameters

To analyze the data obtained, two-factor ANOVA was performed using confidence level = 95 % to validate the significance of the output data as there are two independent factors (infill density and printing speed parameters) in the experiment [24,25]. The observed data were

Table 2
Printing parameters settings.

Parameters Settings	Values
Nozzle temperature (°C)	240
Bed temperature (°C)	70
Infill density (%)	50,60,70,80
Printing speed (mm/s)	20,30,40,50,60
Infill pattern	Cubic

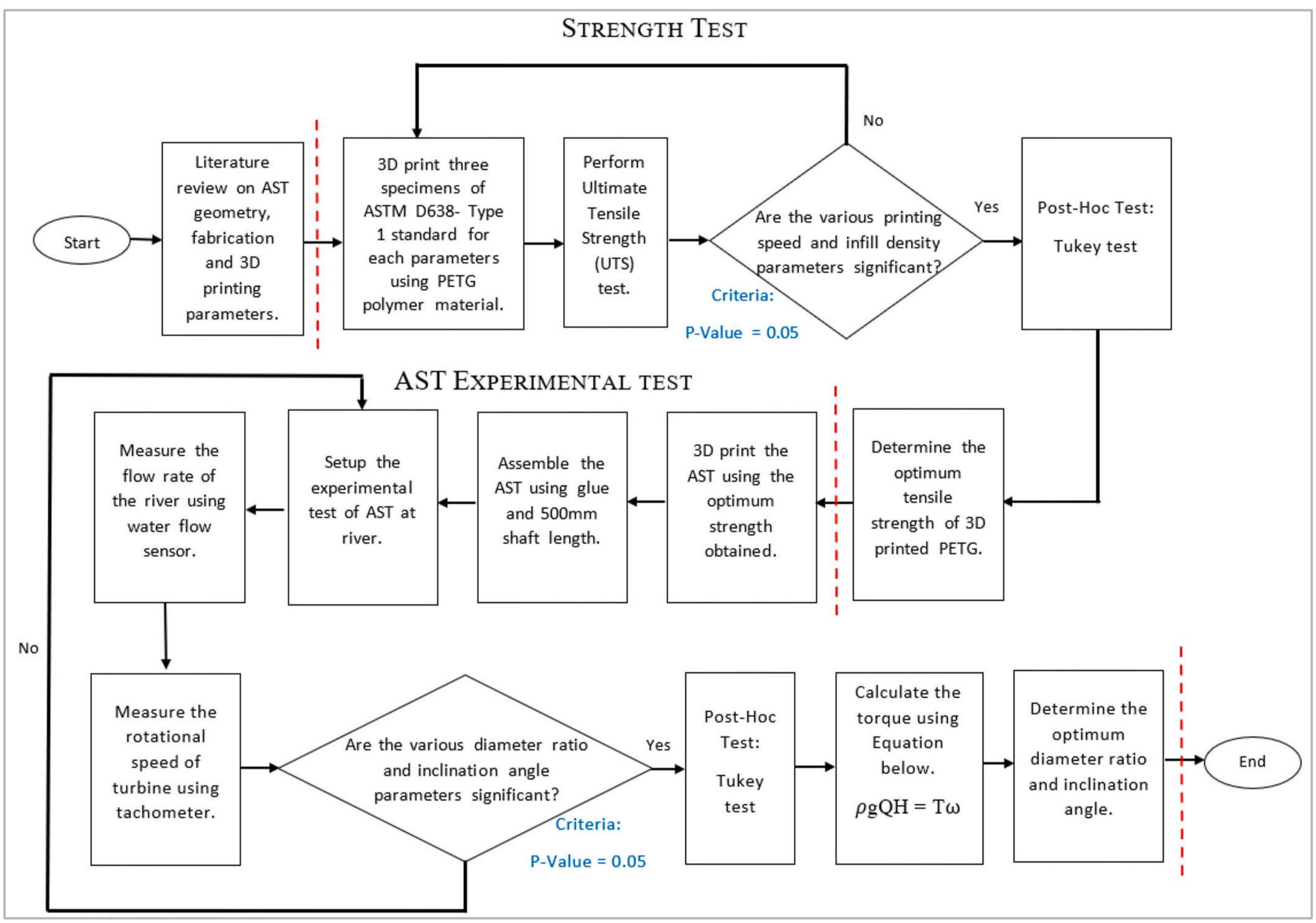

Fig. 2. Flowchart of Experimental Test of strength for 3D printed Archimedean Screw Turbine using PETG material.

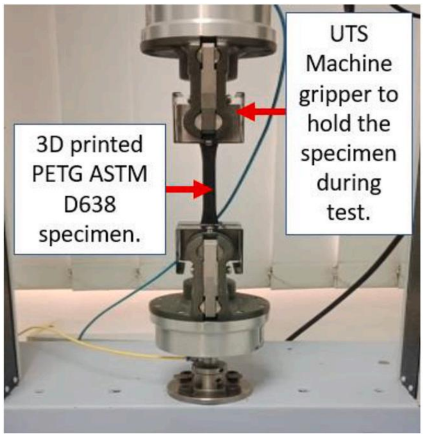

Fig. 3. Ultimate Tensile Test of ASTM D638 Type 1 for 3D printed PETG.

tabulated based on Table 3.

Then, after ANOVA was performed, post-hoc test was performed to further investigate the interactions between the significant factors at confidence level = 95 %. Tukey test was conducted in this experimental work using Minitab software.

3.1.3. Determine the optimum infill density and 3D printing speed parameters

From the data obtained through the UTS experimental test, it is important to determine which parameters need to be used to fabricate the AST. To develop AST model, it is necessary to apply the optimum 3D printing parameters to fabricate the turbine to ensure the AST's strength is sufficient.

3.2. AST experimental test

AST experimental test was conducted to study the feasibility of 3D printed PETG to generate sufficient torque utilizing low water flow rate at Pusu river. Details of the work was discussed in below.

3.2.1. Experimental setup for 3D printed PETG Archimedean Screw Turbine (AST) test to obtain rotational speed of AST

Three different AST's diameter ratio were designed using Solidworks software and later, the turbines were printed by using the optimum 3D printing parameters obtained. Detail parameters of the AST was shown in Fig. 4.

From Fig. 4, it can be seen that details parameters of AST used in this experimental test. Three different AST parameters were designed which each designed have different diameter ratio (0.36, 0.4 and 0.44). After the turbines were completely printed, the screw turbine were glued and assembled with the 500 mm shaft length. After the turbine was completely printed, the screw turbine was glued and assembled with the 500 mm shaft length. Next, to conduct the AST's experimental test,

Table 3
Data for two factor experimental design for UTS test.

	Printing Speed (Factor B)				
Infill Density (Factor A)	20 rpm	30 rpm	40 rpm	50 rpm	60 rpm
50 %	y_{111}, …,y_{11n}	y_{121}, …, y_{12n}	y_{131}, …, y_{13n}	y_{141}, …, y_{14n}	y_{151}, …, y_{15n}
60 %	y_{211}, …, y_{21n}	y_{221}, …, y_{22n}	y_{231}, …, y_{23n}	y_{241}, …, y_{24n}	y_{251}, …, y_{25n}
70 %	y_{311}, …, y_{31n}	y_{321}, …, y_{32n}	y_{331}, …, y_{33n}	y_{341}, …, y_{34n}	y_{351}, …, y_{35n}
80 %	y_{411}, …, y_{41n}	y_{421}, …, y_{42n}	y_{431}, …, y_{43n}	y_{441}, …, y_{44n}	y_{451}, …, y_{45n}

location of the experimental area was selected as shown in Fig. 5. In this work, Pusu river was selected to carried out the AST experimental test as currently, this river is facing sand sediments issue which cause the depth of river to be shallow [26]. Due to this issue, the flow rate of river also being affected which lead to the low water flow rate of river.

Next, before the rotational speed of the turbine data can be taken, water flow rate of the river was measured using calibrated water flow sensor. Process to measure the flow rate of water is shown in Fig. 6.

Fig. 6(a) shows the process to measure the water flow rate of Pusu river using water flow sensor while Fig. 6(b) illustrates the result of water flow rate of Pusu river obtained from the measurement process. From Fig. 6 (b), the results indicates that water flow rate measurement of Pusu River for day 1, day 2 and day 3 were 8.8L/min, 8.8L/min and 6.7L/min in respect. Through this water flow rate measurement, it can be stated that Pusu River water flow rate has similarity with Sarawak River, which both rivers have low water flow rate. Based on research work conducted by Lee and Lee [2], they tested their AST using minimum water flow rate of Sarawak River at 20L/min. Since the water flow rate of Pusu River is slightly lower than Sarawak River, it can be said that this AST model are feasible to be applied at Sarawak River. After the flow of the water was measured, experimental test was set up as shown in Fig. 7.

Fig. 7 (a) illustrates AST schematic setup to carried out the experimental test while Fig. 7 (b) shows the details parameters setup used to conduct the AST works. Then, for Fig. 7 (c), it illustrates the AST experimental setup conducted at inclined angle while Fig. 7 (d) shows the experimental setup of AST at 0° inclination angle. Next, by using the calibrated digital laser tachometer, the rotational speed of rotating turbine was measured. During the experimental test, 16 samples of AST's rotational speed data were collected. This data collection step was repeated for each turbine's diameter ratio (0.36, 0.40 & 0.44) to obtain the median of the rotational speed.

3.2.2. Data analysis using the two-factor Analysis of Variance (ANOVA) and tukey test for diameter ratio and inclination angle parameters

To analyze the data obtained, Two-factor ANOVA was performed using Minitab software using confidence level = 95 % to validate the significance of the output data. This test was conducted by investigating two factors which were diameter ratio and inclination angle of AST. The collected data were tabulated based on Table 4.

After ANOVA was performed, post-hoc test was performed to further investigate the interactions between the significant factors at confidence level = 95 %. Tukey test was conducted in this experimental work using Minitab software.

3.2.3. Torque calculation

From the AST experimental result, the readings that display on tachometer is the rotational speed in rotation per minute (rpm) unit. Hence, the calculation of torque using rotational speed output can be calculated using Eq. (1) [2].

$$\rho g Q H = T\omega \quad (1)$$

Where ρ = density of water (998kg/m^3), g = gravitational acceleration (9.81 m/s^2), Q = volume flow rate (m^3/s) and H = elevation of the system (m), T = torque generated (N/m) and ω = rotation of the turbine shaft (rad/s).

3.2.4. Determine the optimum diameter ratio and inclination angle parameters

From the data obtained through the AST experimental test, it is important to determine which parameters need to be used to obtain high torque to generate sufficient clean energy.

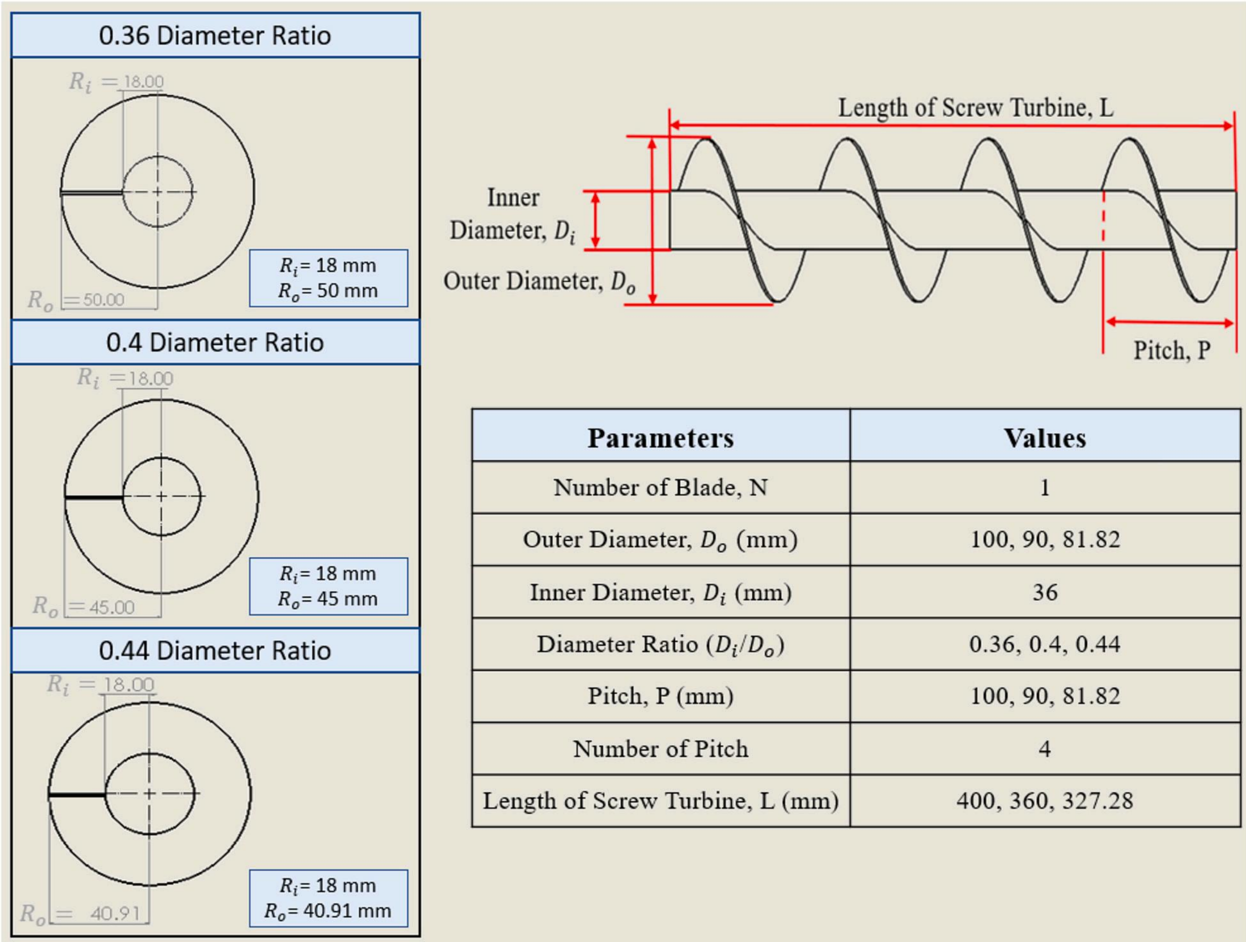

Parameters	Values
Number of Blade, N	1
Outer Diameter, D_o (mm)	100, 90, 81.82
Inner Diameter, D_i (mm)	36
Diameter Ratio (D_i/D_o)	0.36, 0.4, 0.44
Pitch, P (mm)	100, 90, 81.82
Number of Pitch	4
Length of Screw Turbine, L (mm)	400, 360, 327.28

Fig. 4. Design Parameters of AST for 0.36, 0.4 and 0.44 Diameter ratio.

(a) Pusu River Google Map (b) Pusu River Live Location

Fig. 5. Location to conduct AST's experimental test.

3.3. *Assumption towards limitation encounter during experimental test*

During experimental test, the below assumption was taken.

- Overall, the water flow rate of the river is assumed to be consistent during the whole time of the experiment after the data flow rate of water was taken. Based on the reading the maximum difference is between ± 0.8 L/min per day which is an insignificant difference in the water flow rate.

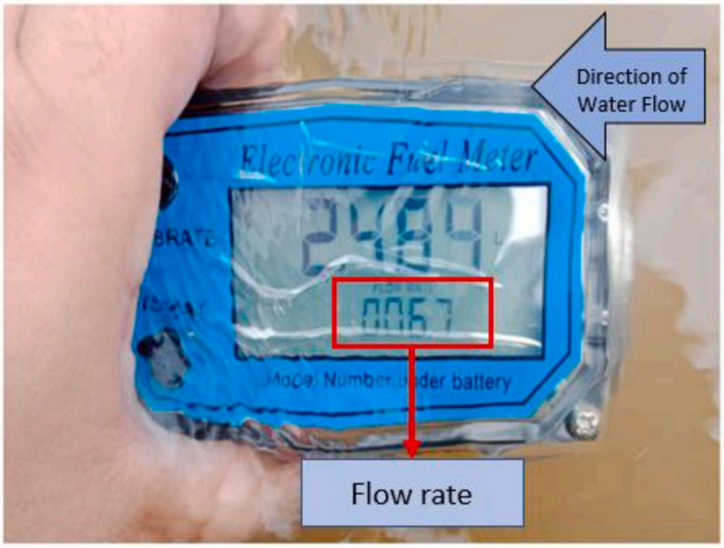

(a) Process to measure Pusu's river flow rate

Day	Date	Flow rate (L/min)			Average Flow Rate (L/min)
1	3 September 2024	8.8	9.0	8.6	8.8
2	6 September 2024	8.8	9.2	8.5	8.8
3	13 September 2024	7.1	6.7	6.3	6.7

(b) Pusu's river flow rate data for Day 1, Day 2 and Day 3.

Fig. 6. (a) Process to measure water flow rate of Pusu river using water flow sensor and (b) Water flow rate of Pusu's river data for Day 1, Day 2 and Day 3.

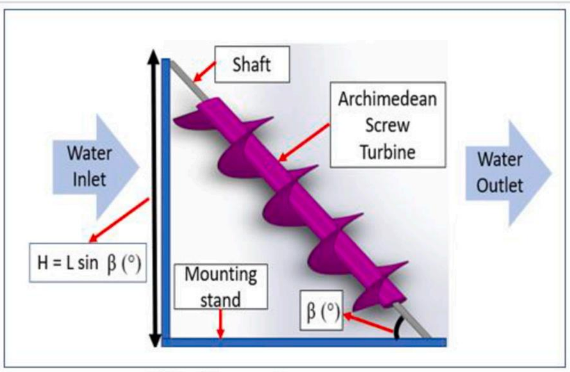

(a) Schematic setup

Parameters	Value
Average Flow Rate, Q (L/min)	8.8, 6.7
Inclination Angle, β (°)	0°,10°,20°,30°
Height of Elevation System, H (m)	$\beta = 0°$, $H = {D_o}/{2}$, $\beta > 0°$, $H = L \sin \beta$
Length of shaft, L (m)	0.5

(b) Experimental parameters setup

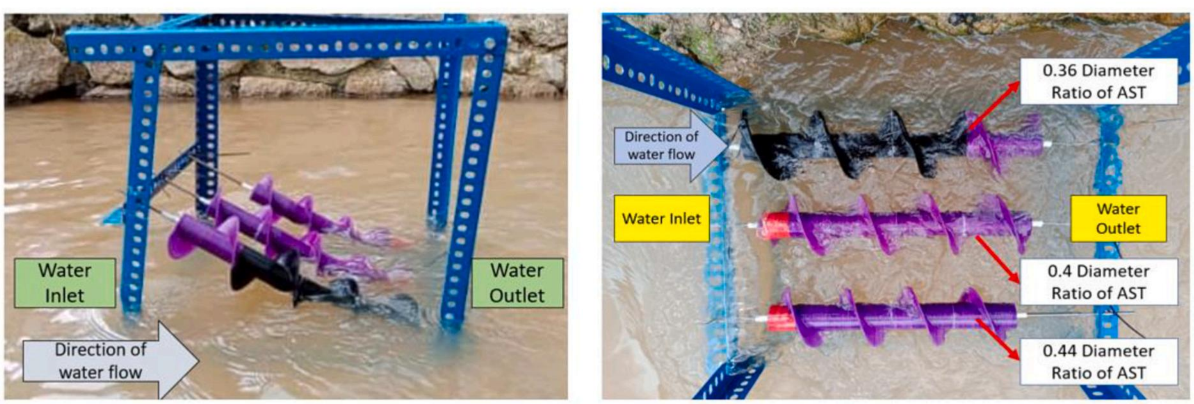

(c) Experimental setup of AST at inclined angle (d) Experimental setup of AST at 0° inclined angle

Fig. 7. (a) Schematic setup for AST Experimental test (b) AST parameters setup (c) Experimental setup of AST at inclined angle (d) Experimental setup of AST at 0° inclination angle.

4. Results and discussion

4.1. Strength test results and discussion

Ultimate Tensile Test (UTS) test was performed to investigate the tensile strength of PETG polymer material. Fig. 8 shows the final outcome of 3D printed PETG after UTS experiment.

Fig. 8(a) shows the fractured 3D printed PETG tensile specimens (physical outcome from UTS test experiment) while Fig. 8(b) illustrates UTS experimental test results for printing parameters of 80 % infill

Table 4
Data for two factor experimental design for AST experimental test.

Diameter Ratio (Factor A)	Inclination Angle (Factor B) 0°	10°	20°	30°
0.36	$y_{111}, \ldots, y_{11n}$	$y_{121}, \ldots, y_{12n}$	$y_{131}, \ldots, y_{13n}$	$y_{141}, \ldots, y_{14n}$
0.4	$y_{211}, \ldots, y_{21n}$	$y_{221}, \ldots, y_{22n}$	$y_{231}, \ldots, y_{23n}$	$y_{241}, \ldots, y_{24n}$
0.44	$y_{311}, \ldots, y_{31n}$	$y_{321}, \ldots, y_{32n}$	$y_{331}, \ldots, y_{33n}$	$y_{341}, \ldots, y_{34n}$

density and 20 mm/s printing speed. From Fig. 8(b), the average tensile strength of the specimen is 36.5995 MPa.

Fig. 9 illustrates the trend of the graph of tensile strength of 3D printed PETG (MPa) by varying infill density (%) and printing speed (mm/s). From the graph, the optimum tensile strength is 37.10 MPa which was achieved using parameters of infill density of 80 % and printing speed of 20 mm/s. This tensile strength using 3D printed PETG polymer is sufficient in turbine application. This is because in wind turbine application, 3D printed PLA polymer [27] have minimum tensile strength of 26.989 MPa [28].

From Fig. 9, the trends of the graph indicate that increasing of the infill density will also increase the strength. This is because there is direct correlation between an increase infill density and a decrease in the porosity level within the specimen [29]. According to Karad et al. [29] the main cause of failure in the Fused Deposition Modelling is porosity. Thus, the greater the porosity, there is high chance of the failure can be formed from large pores and pore clusters. Due to this, at infill density of 80 %, less pore was been created compared to the infill density of 40 % which cause the high strength of the specimen.

Besides, from the graph, it can be seen that decreasing of printing speed leads to increasing the strength of the 3D printed PETG. This is because at the higher printing speed, porosity and void is expected to be increased within the material [30]. As reported by Loskot et al. [31], the possible reason is because at the higher speed, no sufficient material has been supplied through nozzle. Therefore, the extruded path is thinner which cause the molten material at the extruded path is not overlap. Due to this, porosity and void are induced at the higher speed. Kim et al. [30] mentions that voids can adversely affect the interfacial strength between the neighboring paths, which could have a negative impact on mechanical properties of the finished product, which comprises ultimate tensile stress/Young's modulus. Similar findings were reported in the work of Pazhamannil et al. [32], which correlated large voids induced at rapid printing speed to a reduction in the printed PLA's mechanical

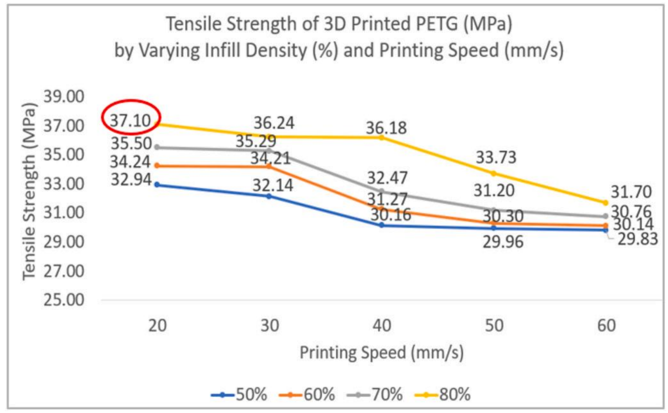

Fig. 9. Tensile strength of 3D printed PETG (MPa) by varying infill density (%) and printing speed (mm/s).

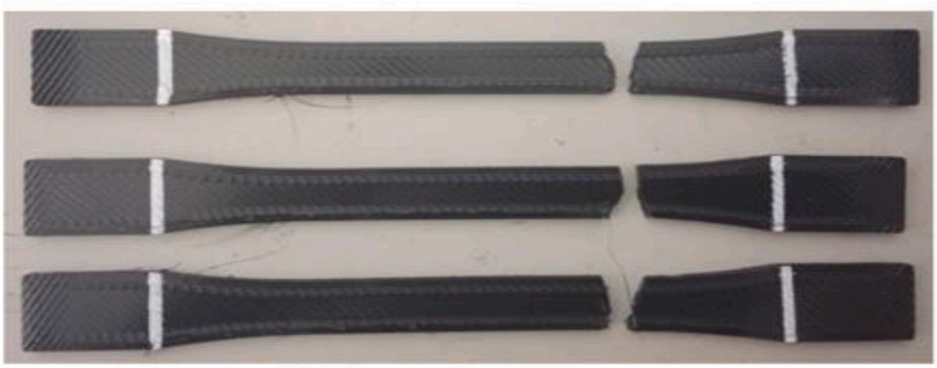

(a) Physical outcome

Name / Parameters / Unit	Young Modulas Force 10 – 20 N MPa	Tensile Strength Calc. at Entire Areas MPa	Yield Strength 0.2 % MPa	Max_Force Calc. at Entire Areas N
41	1038.37	36.5995	34.6852	1522.54
Average	1038.37	36.5995	34.6852	1522.54
Standard Deviation	-.-	-.-	-.-	-.-
Maximum	1038.37	36.5995	34.6852	1522.54
Minimum	1038.37	36.5995	34.6852	1522.54
Range	0.00000	0.00000	0.00000	0.00000
Median	1038.37	36.5995	34.6852	1522.54
Variation	-.-	-.-	-.-	-.-
3Sigma	-.-	-.-	-.-	-.-

(b) UTS experimental test result

Fig. 8. Final outcome of UTS experimental test.

strength. The ANOVA test was carried out to validate the significance of the infill density and printing speed parameters on tensile strength output.

Fig. 10 illustrates the results of two factor ANOVA analysis for tensile strength of 3D printed PETG. The calculation was carried out at the significance level of P-value = 0.05 using Minitab software. From Fig. 10, it can be stated that infill density and printing speed parameters are significant towards the tensile strength output as P-value for infill density and printing speed are 0.000. Since the parameters are significant, further investigation towards the infill density and printing speed factors were performed using Post Hoc Tukey test using Minitab software. Fig. 11 illustrates the post hoc Tukey test results for infill density and printing speed.

Fig. 11(a) illustrates tukey test results for infill density while Fig. 11 (b) shows tukey test results for printing speed. From Fig. 11(a), it can be seen that all the pairwise are significant excepts interaction pairwise of infill density (%) of 60.00–50.00 and 70.00–60.00. This is because both the parameters have the p-value above 0.05. Subsequently, in Fig. 11(b), tukey test results shows the all the interactions are significant except for interactions of printing speed (mm/s) for pairwise 30-20, 50- 40 and 60-50. This is because the p-value of the above printing speed are more than 0.05.

4.2. AST experimental test results and discussion

Further investigation of the 3D printed models was studied through the Archimedean Screw Turbine's capability to generate torque using low water flow rate of Pusu river. Fig. 12(a) and (b) and (c) show rotational speed of the turbine at different diameter ratio (0.36, 0.4 and 0.44) and inclination angle (0°,10°,20° and 30°) at Day 1, Day 2 and Day 3 respectively. From Fig. 12, it shows that the high water flow rate will have high turbines' rotational speed at the three diameter ratios investigated. Furthermore, the maximum rotational speed of the turbine at different diameter ratio was summarized at Table 5.

From Tables 5 and it can be stated that at all diameter ratio, at 8.8L/min water flow rate, the turbine rotates at high speed compared to water flow rate of 6.7L/min. This is because an increase in the water flow rate will lead to increasing in the kinetic energy, which cause the turbine to rotate faster. The result is aligned with Lee and Lee [2] research which reported that increase in water flow rate causing an increase in rotational speed of turbine.

From Table 5 also, increasing in diameter ratio led to increasing the rotational speed. At all water flow rates, 0.44 diameter ratio rotates at high speed followed by 0.4 and 0.36 diameter ratio respectively. Therefore, an increase in diameter ratio will decrease the outer diameter blade surface. Thus, it will cause a decrease of the volume of the water trapped between the blades [33]. Hence, the turbine can rotate faster due to the less volume of water trapped between the blades. However, a decrease in diameter ratio, the outer diameter blade surface will increase, causing the increase of the volume of water trapped between the blades [33]. Due to this, the turbine rotates slowly as the heavier weight of the water trapped between the blades.

From Fig. 12(a) and (b) and (c), it can be seen that, at all water flow rate and diameter ratio of the turbine, it indicates that at 0° inclination angle, the turbine rotated at the slowest rotation speed while at 30° inclination angle, the turbine rotated at the highest rotation speed. This is because at the inclination angle of 0°, there is absence of the hydrostatic force. Therefore, the rotations of the screw turbine only depend on the kinetic force from the flowing water [34]. At the 10°,20° and 30° angle inclination, the turbine rotated more faster than 0° due to the occurrence of hydrostatic force. Hydrostatic force occurs when there is difference in a head level between water inlet (higher elevation) and water outlet (lower elevation) due to the assistance of the gravity to push the water trapped between the blade to the water outlet.

Analysis of Variance

Source	DF	Adj SS	Adj MS	F-Value	P-Value
Infill Density	3	129.76	43.254	32.14	0.000
Printing Speed	4	174.43	43.609	32.41	0.000
Infill Density*Printing Speed	12	20.27	1.689	1.26	0.282
Error	40	53.82	1.346		
Total	59	378.29			

Fig. 10. Results of two factor ANOVA analysis for tensile strength of 3D printed PETG.

Two factor Analysis of Variance (ANOVA) was used to validate the significance of the two variable parameters (diameter ratio and inclination angle). The summary of results of two factor ANOVA using Minitab software are illustrates in Fig. 13.

Based on Fig. 13(a), (b) and (c), the results show that the P-value for diameter ratio and inclination angle are 0.000 and 0.000 in respect for all water flow rate. Thus, it indicates that diameter ratio and inclination angle are significant parameters in this work as the p-value is less than 0.05. Since the diameter ratio and inclination angle are significance towards the rotational speed output, further analysis was carried out using Tukey test. The results of the Tukey test for diameter ratio and inclination angle for water flow rate of 8.8L/min (Day 1), 8.8L/min (Day 2) and 6.7L/min (Day 3) are shown in Fig. 14.

From Fig. 14, it can be seen that all the pairwise for all water flow rate are significant excepts for the interaction pairwise of inclination angle (°) of 30-20 for day 1 and interaction pairwise of inclination angle (°) of 20-10 for day 3. This is because the p-value of the above pairwise are 0.276 and 0.126 which is larger than the p-value of 0.05.

By using Equation (1), the torque value can be calculated by substituting the data within Fig. 7(b). Torque data for river water flow rate 8.8L/min/8.8L/min and 6.7L/min are shown in Fig. 15(a),(b) and (c) respectively.

From Fig. 15(a) and (b) and (c), it can be observed that decreasing in diameter ratio led to an increase in the torque value. From this graph, at all water flow rates and inclination angle, it can be concluded that 0.36 diameter ratio generated the highest torque while 0.44 generated the lowest torque. Results from this research work are similar to the research outcome by Erinofiardi et al. [5] which stated that the increase the rotational speed of the turbine causing decrease in torque. From Fig. 15 (a), (b) and (c), it can be stated that 30° inclination angle is the optimum inclination angle as it generated the highest torque. The result is aligned with research [6,7] which reported that 30° is the common angle used to install the turbine. Based on the experimental results data of Lee and Lee [2], they varied the inclination at high inclination angle which are 30°, 45°,60°,75° and 90° in their work and the finding indicates that 30° angle is generating the second highest torque output.

5. Conclusion

In this work, a pico-hydro power turbine (AST) made using PETG material was designed to work in low water flow rate river for clean energy generation. Ultimate Tensile Strength (UTS) test was carried out to investigate the tensile strength of the 3D printed PETG polymer material. Two variable 3D printing parameters were utilized, infill density and printing speed. The final outcome indicates that 80 % infill density and 20mm/s printing speed were the optimum parameters to obtain the highest tensile strength at 37.10MPa. Three prototypes with different diameter ratio (0.36,0.4 & 0.44) were designed using SolidWorks software and fabricated using the optimum 3D printing parameters obtained. Experimental test was carried out at Pusu river, Selangor, Malaysia to study the feasibility of 3D printed AST to generate sufficient torque using river flow rate. The average water flow rate of Pusu river are 8.8L/min, 8.8L/min and 6.7L/min, respectively for each day. At the 8.8L/min water flow rate, all the diameter ratio of AST generated high rotational speed of turbine compared to the 6.7L/min flow rate. From the output obtained, it can be stated that at all water flow rates and

(a) Tukey Simultaneous Tests for Differences of Means

Difference of Infill Density Levels	Difference of Means	SE of Difference	Simultaneous 95% CI	T-Value	Adjusted P-Value
60.00% - 50.00%	1.025	0.424	(-0.110, 2.160)	2.42	0.090
70.00% - 50.00%	2.038	0.424	(0.903, 3.173)	4.81	0.000
80.00% - 50.00%	3.982	0.424	(2.846, 5.117)	9.40	0.000
70.00% - 60.00%	1.013	0.424	(-0.122, 2.148)	2.39	0.095
80.00% - 60.00%	2.957	0.424	(1.822, 4.092)	6.98	0.000
80.00% - 70.00%	1.944	0.424	(0.809, 3.079)	4.59	0.000

Individual confidence level = 98.94%

(b) Tukey Simultaneous Tests for Differences of Means

Difference of Printing Speed Levels	Difference of Means	SE of Difference	Simultaneous 95% CI	T-Value	Adjusted P-Value
30 - 20	-0.476	0.474	(-1.829, 0.877)	-1.00	0.852
40 - 20	-2.424	0.474	(-3.777, -1.071)	-5.12	0.000
50 - 20	-3.647	0.474	(-5.000, -2.294)	-7.70	0.000
60 - 20	-4.340	0.474	(-5.693, -2.988)	-9.17	0.000
40 - 30	-1.948	0.474	(-3.301, -0.595)	-4.11	0.002
50 - 30	-3.171	0.474	(-4.524, -1.819)	-6.70	0.000
60 - 30	-3.865	0.474	(-5.217, -2.512)	-8.16	0.000
50 - 40	-1.224	0.474	(-2.576, 0.129)	-2.58	0.093
60 - 40	-1.917	0.474	(-3.270, -0.564)	-4.05	0.002
60 - 50	-0.693	0.474	(-2.046, 0.660)	-1.46	0.591

Individual confidence level = 99.32%

Fig. 11. Tukey test results (a) Infill Density (b) Printing Speed.

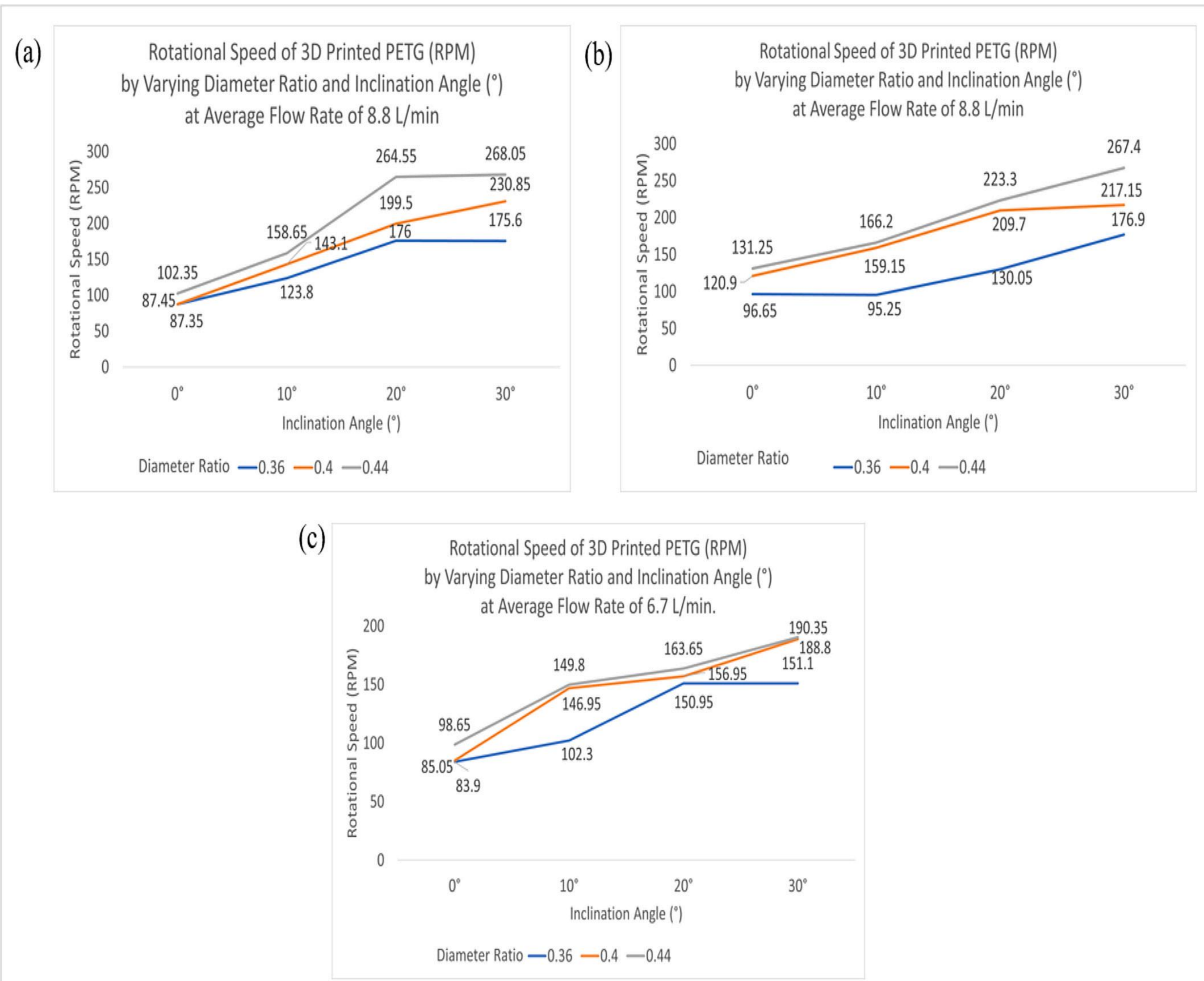

Fig. 12. Rotational speed of 3D printed PETG for various diameter ratio at average water flow rate of 8.8L/min (a), 8.8L/min (b) and 6.7L/min (c).

diameter ratio, at 30° inclination angle, turbine rotate rapidly while at 0° inclination angle, the turbine rotates slowly. From the experimental results, at all water flow rate and inclination angle, it can be observed that 0.44 diameter ratio, the AST rotated at maximum rotational speed of 268.05 rpm. However, from the torque calculated, at all water flow rate and inclination angle, 0.36 diameter ratio, the AST generated the

Table 5
Maximum Rotational speed of turbine at 0.36, 0.4 and 0.44 diameter ratio.

Day	Flow rate (L/min)	RPM of 0.36 diameter ratio at β = 30°	RPM of 0.40 diameter ratio at β = 30°	RPM of 0.44 diameter ratio at β = 30°
1	8.8	175.6	230.85	268.05
2	8.8	176.9	217.15	267.4
3	6.7	151.1	188.8	190.35

maximum torque at 0.0195 N.m while 0.44 diameter ratio, the AST generated maximum torque at 0.0128 N.m. From the torque output, it can be observed that 0.36 diameter ratio generated more torque compared to the 0.44 diameter ratio. This is because torque and rotational speed is inversely proportional to each other which increase in rotational speed of the turbine will cause decrease in torque. From the output results, 3D printed AST utilizing PETG material are able to generate sufficient torque for pico-hydro energy generation for rural electrification in Malaysia. To ensure this AST model can be applied in

(a) Analysis of Variance

Source	DF	Adj SS	Adj MS	F-Value	P-Value
Diameter Ratio	2	96888	48444	76.16	0.000
Inclination Angle	3	578021	192674	302.92	0.000
Diameter Ratio*Inclination Angle	6	30497	5083	7.99	0.000
Error	180	114491	636		
Total	191	819897			

(b) Analysis of Variance

Source	DF	Adj SS	Adj MS	F-Value	P-Value
Diameter Ratio	2	186561	93281	176.03	0.000
Inclination Angle	3	317567	105856	199.76	0.000
Diameter Ratio*Inclination Angle	6	26771	4462	8.42	0.000
Error	180	95385	530		
Total	191	626285			

(c) Analysis of Variance

Source	DF	Adj SS	Adj MS	F-Value	P-Value
Diameter Ratio	2	41443	20722	20.36	0.000
Inclination Angle	3	219530	73177	71.89	0.000
Diameter Ratio*Inclination Angle	6	18813	3135	3.08	0.007
Error	180	183228	1018		
Total	191	463014			

Fig. 13. Summary of ANOVA results for water flow rate of Pusu river at (a) 8.8L/Min, (b) 8.8L/min and (c) 6.7L/min.

Day	Flow rate (L/min)	Tukey test result for diameter ratio	Tukey test result for inclination angle
1	8.8	see below	see below
2	8.8	see below	see below
3	6.7	see below	see below

Day 1, 8.8 — Tukey test result for diameter ratio

Tukey Simultaneous Tests for Differences of Means

Difference of Diameter Ratio Levels	Difference of Means	SE of Difference	Simultaneous 95% CI	T-Value	Adjusted P-Value
0.40 - 0.36	21.75	4.46	(11.22, 32.28)	4.88	0.000
0.44 - 0.36	54.65	4.46	(44.12, 65.18)	12.26	0.000
0.44 - 0.40	32.90	4.46	(22.37, 43.43)	7.38	0.000

Individual confidence level = 98.07%

Day 1, 8.8 — Tukey test result for inclination angle

Tukey Simultaneous Tests for Differences of Means

Difference of Inclination Angle Levels	Difference of Means	SE of Difference	Simultaneous 95% CI	T-Value	Adjusted P-Value
10 - 0	53.74	5.15	(40.38, 67.10)	10.44	0.000
20 - 0	124.97	5.15	(111.61, 138.33)	24.27	0.000
30 - 0	134.25	5.15	(120.89, 147.61)	26.08	0.000
20 - 10	71.23	5.15	(57.87, 84.59)	13.84	0.000
30 - 10	80.51	5.15	(67.15, 93.87)	15.64	0.000
30 - 20	9.28	5.15	(-4.08, 22.64)	1.80	0.276

Individual confidence level = 98.98%

Day 2, 8.8 — Tukey test result for diameter ratio

Tukey Simultaneous Tests for Differences of Means

Difference of Diameter Ratio Levels	Difference of Means	SE of Difference	Simultaneous 95% CI	T-Value	Adjusted P-Value
0.40 - 0.36	47.83	4.07	(38.22, 57.44)	11.75	0.000
0.44 - 0.36	75.46	4.07	(65.85, 85.07)	18.54	0.000
0.44 - 0.40	27.63	4.07	(18.02, 37.24)	6.79	0.000

Individual confidence level = 98.07%

Day 2, 8.8 — Tukey test result for inclination angle

Tukey Simultaneous Tests for Differences of Means

Difference of Inclination Angle Levels	Difference of Means	SE of Difference	Simultaneous 95% CI	T-Value	Adjusted P-Value
10 - 0	25.68	4.70	(13.49, 37.88)	5.47	0.000
20 - 0	74.78	4.70	(62.59, 86.98)	15.91	0.000
30 - 0	104.00	4.70	(91.80, 116.19)	22.13	0.000
20 - 10	49.10	4.70	(36.90, 61.29)	10.45	0.000
30 - 10	78.31	4.70	(66.12, 90.51)	16.67	0.000
30 - 20	29.21	4.70	(17.02, 41.41)	6.22	0.000

Individual confidence level = 98.98%

Day 3, 6.7 — Tukey test result for diameter ratio

Tukey Simultaneous Tests for Differences of Means

Difference of Diameter Ratio Levels	Difference of Means	SE of Difference	Simultaneous 95% CI	T-Value	Adjusted P-Value
0.40 - 0.36	15.39	5.64	(2.07, 28.71)	2.73	0.019
0.44 - 0.36	35.87	5.64	(22.55, 49.19)	6.36	0.000
0.44 - 0.40	20.48	5.64	(7.16, 33.80)	3.63	0.001

Individual confidence level = 98.07%

Day 3, 6.7 — Tukey test result for inclination angle

Tukey Simultaneous Tests for Differences of Means

Difference of Inclination Angle Levels	Difference of Means	SE of Difference	Simultaneous 95% CI	T-Value	Adjusted P-Value
10 - 0	51.44	6.51	(34.54, 68.34)	7.90	0.000
20 - 0	65.79	6.51	(48.89, 82.69)	10.10	0.000
30 - 0	92.99	6.51	(76.09, 109.89)	14.28	0.000
20 - 10	14.35	6.51	(-2.55, 31.25)	2.20	0.126
30 - 10	41.55	6.51	(24.65, 58.45)	6.38	0.000
30 - 20	27.20	6.51	(10.30, 44.10)	4.18	0.000

Individual confidence level = 98.98%

Fig. 14. Tukey test results for diameter ratio and inclination angle for flow rate of 8.8 L/min (Day 1), 8.8L/min (Day 2) and 6.7L/min (Day 3).

Fig. 15. Torque of 3D printed PETG for various diameter ratio at average water flow rate of 8.8 L/min (a), 8.8 L/min (b) and 6.7 L/min (c).

Sarawak River, the turbine must have a proper mounting stand for each model. A proper mounting stand need to be developed to ensure the turbine can hold the AST as expected. In the future works, it is recommended to perform future investigation different materials for AST fabrication utilizing additive manufacturing technology as 3D printing manufacturing creates less material waste which is good for the environment.

CRediT authorship contribution statement

Nuranisa Suhada binti Abd Rahim: Writing – original draft, Visualization, Investigation, Formal analysis, Data curation. **Chuan Choong Yang:** Writing – review & editing, Validation, Supervision, Methodology, Conceptualization. **Nor Aiman Sukindar:** Conceptualization.

Declaration of competing interest

The authors declare that they have no known competing financial interests or personal relationships that could have appeared to influence the work reported in this paper.

Data availability

Data will be made available on request.

References

[1] N. Julai, Y.W.Y. Buswig, Hybrid renewable system based pumped energy storage for the electrification of rural areas, in: 13th International UNIMAS Engineering Conference (EnCon), 2020, https://doi.org/10.1109/encon51501.2020.9299334.
[2] M.D. Lee, P.S. Lee, Modelling the energy extraction from low-velocity stream water by small scale archimedes screw turbine, J. King Saud Univ.- Eng. Sci. 35 (5) (2021) 319–326, https://doi.org/10.1016/j.jksues.2021.04.006.
[3] T.T.H. Nguyen, G.Q. Phan, T.K. Tran, H.M. Bui, The role of renewable energy technologies in enhancing human development: empirical evidence from selected countries, Case Stud. Chem. Environ. Eng. 8 (2023) 100496, https://doi.org/10.1016/j.cscee.2023.100496.
[4] A. YoosefDoost, W. Lubitz, Archimedes screw turbines: a sustainable development solution for green and renewable energy generation—a review of potential and design procedures, Sustainability 12 (18) (2020) 7352, https://doi.org/10.3390/su12187352.
[5] N. Erinofiardi, A. Nuramal, P. Bismantolo, A. Date, A. Akbarzadeh, A.K. Mainil, A. F. Suryono, Experimental study of screw turbine performance based on different angle of inclination, Energy Proc. 110 (2017) 8–13, https://doi.org/10.1016/j.egypro.2017.03.094.
[6] I. Syam, M.I. Maulana, A. Syuhada, Design and performance of archimedes single screw turbine as micro hydro power plant with flow rate debit variations (case study in air dingin, samadua - south aceh), Jurnal Inotera 4 (1) (2019) 13, https://doi.org/10.31572/inotera.vol4.iss1.2019.id71.
[7] M.I. Maulana, A. Syuhada, R. Kurniawan, Experimental study on the effect of flow rate on the performance of two-blade archimedes screw turbine. https://semarakilmu.com.my/journals/index.php/fluid_mechanics_thermal_sciences/article/view/3483, 2019.
[8] G. Nagel, Archimedian Screw Pump Handbook : Fundamental Aspects of the Design and Operation of Water Pumping Installations Using Archimedian Screw Pumps, RITZ-Pumpenfabrik OHG, 1968.
[9] N. S. B. A. Rahim, C. C. Yang, N. F. N. B. Mamat, Optimizing an archimedean screw turbine (AST) at low water flow velocity for clean energy generation, Proceeding of 6th International Conference on Advances in Manufacturing and Materials Engineering (ICAMME) 2024, Lecture Notes in Mechanical Engineering, Springer.
[10] G.O.V. Energy, The 21st century archimedes screw: new materials and manufacturing techniques enable the turbine's highest-ever measured efficiency. https://www.energy.gov/eere/water/articles/21st-century-archimedes-screw-new-materials-and-manufacturing-techniques-enable, 2021.
[11] W. Yan, H. Zhang, Z. Jiang, K. Hon, Multi-objective optimization of arc welding parameters: the trade-offs between energy and thermal efficiency, J. Clean. Prod. 140 (2016) 1842–1849, https://doi.org/10.1016/j.jclepro.2016.03.171.
[12] E. Karayel, Y. Bozkurt, Additive manufacturing method and different welding applications, J. Mater. Res. Technol. 9 (5) (2020) 11424–11438, https://doi.org/10.1016/j.jmrt.2020.08.039.
[13] M.R. Khosravani, T. Reinicke, On the environmental impacts of 3D printing technology, Appl. Mater. Today 20 (2020) 100689, https://doi.org/10.1016/j.apmt.2020.100689.
[14] M.A. Islam, M.H. Mobarak, M.I.H. Rimon, M.Z.A. Mahmud, J. Ghosh, M.M. S. Ahmed, N. Hossain, Additive manufacturing in polymer research: advances,

synthesis, and applications, Polym. Test. (2024) 108364, https://doi.org/10.1016/j.polymertesting.2024.108364.

[15] K.T. Lee, E. Kim, W. Chu, S. Ahn, Design and 3D printing of controllable-pitch archimedean screw for pico-hydropower generation, J. Mech. Sci. Technol. 29 (11) (2015) 4851–4857, https://doi.org/10.1007/s12206-015-1032-y.

[16] G. Zitti, F. Fattore, A. Brunori, B. Brunori, M. Brocchini, Efficiency evaluation of a ductless archimedes turbine: laboratory experiments and numerical simulations, Renew. Energy 146 (2019) 867–879, https://doi.org/10.1016/j.renene.2019.06.174.

[17] D.M. Nieto, M. Alonso-García, M. Pardo-Vicente, L. Rodríguez-Parada, Product design by additive manufacturing for water environments: study of degradation and absorption behavior of PLA and PETG, Polymers 13 (7) (2021) 1036, https://doi.org/10.3390/polym13071036.

[18] M.A. Mazlan, M.A. Anas, N.A.N. Izmin, A.H. Abdullah, Effects of infill density, wall perimeter and layer height in fabricating 3D printing products, Materials 16 (2) (2023) 695, https://doi.org/10.3390/ma16020695.

[19] S.S. Ambati, R. Ambatipudi, Effect of infill density and infill pattern on the mechanical properties of 3D printed PLA parts, Mater. Today Proc. 64 (2022) 804–807, https://doi.org/10.1016/j.matpr.2022.05.312.

[20] J. Maszybrocka, M. Dworak, G. Nowakowska, P. Osak, B. Łosiewicz, The influence of the gradient infill of PLA samples produced with the FDM technique on their mechanical properties, Materials 15 (4) (2022) 1304, https://doi.org/10.3390/ma15041304.

[21] D. Farbman, C. McCoy, Materials testing of 3D printed ABS and PLA samples to guide mechanical design, Materials; Biomanufacturing; Properties, Applications and Systems; Sustainable Manufacturing ume 2 (2016), https://doi.org/10.1115/msec2016-8668.

[22] L. Miazio, Impact of print speed on strength of samples printed in FDM technology, Agricultural Eng. 23 (2) (2019) 33–38, https://doi.org/10.1515/agriceng-2019-0014.

[23] M. Hsueh, C. Lai, S. Wang, Y. Zeng, C. Hsieh, C. Pan, W. Huang, Effect of printing parameters on the thermal and mechanical properties of 3D-printed PLA and PETG, using fused deposition modeling, Polymers 13 (11) (2021) 1758, https://doi.org/10.3390/polym13111758.

[24] N.S.B.A. Rahim, C.C. Yang, N.D.B. Zulkarnain, N.H.H.B.M. Hanif, Semi-automatic dough weighing machine for enhanced productivity in quality control processes, Intern. Confer. Mecha. Eng. 6 (2024) 251–254, https://doi.org/10.1109/icom61675.2024.10652537.

[25] C.C. Yang, N.F.R.B.N. Hanafi, N.H.H.B.M. Hanif, A.F. Ismail, H. Chang, A novel non-intrusive vibration energy harvesting method for air conditioning compressor unit, Sustainability 13 (18) (2021) 10300, https://doi.org/10.3390/su131810300.

[26] F.A. Razali, M.F. Ayob, Appraisal of cost-effective approaches for the PUSU river rehabilitation, J. Archit. Plan. Construct. Manag. 12 (2) (2022) 40–57, https://doi.org/10.31436/japcm.v12i2.669.

[27] S. A, R.K. S, B. Aljafari, S.B. Thanikanti, Investigations of the performance of 3D printed micro wind turbine composed of PLA material, Heliyon 10 (3) (2024) e25356, https://doi.org/10.1016/j.heliyon.2024.e25356.

[28] N.A. Sukindar, S.I.S. Shaharuddin, S. Kamruddin, A.Z.A. Azhar, C.C. Yang, Comparison study on mechanical properties of 3D printed PLA and pla/aluminium composites using fused deposition modeling technique. https://malaysianjournalofmicroscopy.org/ojs/index.php/mjm/article/view/541, 2022.

[29] A.S. Karad, P.D. Sonawwanay, M. Naik, D.G. Thakur, Experimental study of effect of infill density on tensile and flexural strength of 3D printed parts, J. Eng. Appl. Sci. 70 (1) (2023), https://doi.org/10.1186/s44147-023-00273-x.

[30] S. Kim, V.F. Korolovych, R.L. Muhlbauer, V.V. Tsukruk, 3D-printed polymer packing structures: uniformity of morphology and mechanical properties via microprocessing conditions, J. Appl. Polym. Sci. 137 (44) (2020), https://doi.org/10.1002/app.49381.

[31] J. Loskot, D. Jezbera, R. Loskot, D. Bušovský, A. Barylski, K. Glowka, P. Duda, K. Aniołek, K. Voglová, M. Zubko, Influence of print speed on the microstructure, morphology, and mechanical properties of 3D-printed PETG products, Polym. Test. 123 (2023) 108055, https://doi.org/10.1016/j.polymertesting.2023.108055.

[32] R.V. Pazhamannil, N.K. C, G. P, A. Edacherian, Investigations into the effect of thermal annealing on fused filament fabrication process, Adv. Mater. Proces. Technol. 8 (sup2) (2021) 710–723, https://doi.org/10.1080/2374068x.2021.1946753.

[33] A. Dragomirescu, Design considerations for an archimedean screw hydro turbine, IOP Conf. Ser. Earth Environ. Sci. 664 (1) (2021) 012034, https://doi.org/10.1088/1755-1315/664/1/012034.

[34] S. Waters, G.A. Aggidis, Over 2000 Years in review: revival of the archimedes screw from pump to turbine, Renew. Sustain. Energy Rev. 51 (2015) 497–505, https://doi.org/10.1016/j.rser.2015.06.028.